HHS Public Access

Author manuscript

ACS Appl Mater Interfaces. Author manuscript; available in PMC 2017 October 12.

Published in final edited form as:

ACS Appl Mater Interfaces. 2016 October 12; 8(40): 26630–26637. doi:10.1021/acsami.6b10255.

Cerenkov Radiation Induced Photodynamic Therapy Using Chlorin e6-Loaded Hollow Mesoporous Silica Nanoparticles

Anyanee Kamkaew[1,‡], **Liang Cheng**[1,2,‡], **Shreya Goel**[3,‡], **Hector F. Valdovinos**[4], **Todd E. Barnhart**[4], **Zhuang Liu**[2], and **Weibo Cai**[1,3,4,5,*]

[1]Department of Radiology, University of Wisconsin - Madison, Madison, WI 53705, USA

[2]Institute of Functional Nano & Soft Materials (FUNSOM), Collaborative Innovation Center of Suzhou Nano Science and Technology, Soochow University, Suzhou, Jiangsu 215123, China

[3]Materials Science Program, University of Wisconsin – Madison, Madison, WI 53705, USA

[4]Department of Medical Physics, University of Wisconsin - Madison, Madison, WI 53705, USA

[5]University of Wisconsin Carbone Cancer Centre, Madison, WI, USA

Abstract

Traditional photodynamic therapy (PDT) requires external light to activate photosensitizers for therapeutic purposes. However, the limited tissue penetration of light is still a major challenge for this method. To overcome this limitation, we report an optimized system that uses Cerenkov radiation for PDT by using radionuclides to activate a well-known photosensitizer (Chlorin e6, Ce6). By taking advantage of hollow mesoporous silica nanoparticles (HMSNs) that can intrinsically radiolabel oxophilic zirconium-89 (^{89}Zr, $t_{1/2}$ = 78.4 h) radionuclide, as well as possess great drug loading capacity, Ce6 can be activated by Cerenkov radiation from ^{89}Zr in the same nanoconstruct. *In vitro* cells viability experiments demonstrated dose-dependent cell deconstructions as a function of concentration of Ce6 and ^{89}Zr. *In vivo* studies show inhibition of tumor growth when mice were subcutaneously injected with [^{89}Zr]HMSN-Ce6 and histological analysis of tumor section showed damage to tumor tissues, implying that reactive oxygen species mediated the destruction. This study offers a way to use internal radiation source to achieve deep-seated tumor therapy without using any external light source for future applications.

Graphical abstract

[*]**Corresponding Author:** Department of Radiology, University of Wisconsin, Room 7137, 1111 Highland Ave, Madison, WI 53705-2275. wcai@uwhealth.org. Phone: 608-262-1749. Fax: 608-265-0614.

[‡]**Author Contributions**

These authors contributed equally.

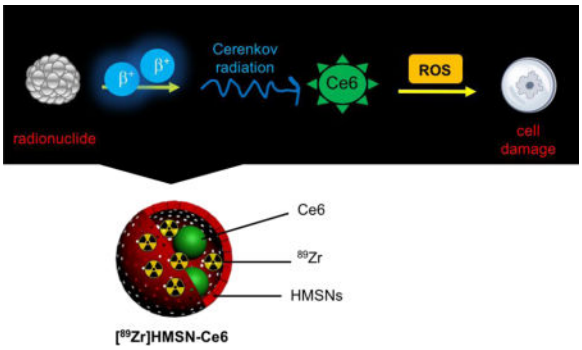

Keywords

Cerenkov radiation; Photodynamic therapy; Hollow mesoporous silica nanoparticles; Chlorin e6; Positron Emission Tomography

Introduction

Photodynamic therapy (PDT) has emerged as a new frontier in biomedical research. In typical PDT, external light is needed to activate photosensitizers (PS) causing cell damage. In this case, treatment of deep-seated tumors is not always effective since most of the light wavelengths (between 400–800 nm) are absorbed and scattered by biological tissues.[1] Thus, a fiber light source is required to treat deep tissues that are endoscopically accessible.[2, 3] A recent advanced approach that attempted to overcome the limitation of tissue penetration of light is the use of chemi/bioluminescent systems that can avoid the external light and use chemi/bioluminescence is an internal light source.[4, 5]

Recently, image-guided therapy has been developed as a tool to optimize therapeutic efficacy.[6–9] In PDT, imaging can provide useful information regarding the size and location of tumors which help to optimize the time window for PDT regimens, as well as monitor the therapeutic efficacy.[10–14] Positron emission tomography (PET) is a powerful whole body imaging technique, with unlimited tissue depth penetration, compared to other optical imaging modalities.[15] Therefore, combination of PET and PDT would be a great candidate to treat cancer. Cerenkov radiation (CR) happens when charged particles, such as β^+ and β^-, generated from radioactive decay emit UV and visible light (250–600 nm) in a broad energy range while traveling through a dielectric medium faster than the speed of light.[16] Here, we hypothesized that CR emitted from radionuclides typically used in PET could serve as a depth-independent light source for photodynamic therapy. Recent advances in technology for detection of low-intensity light have enabled the application of CR as a light source for molecular imaging, either alone or in complexation with energy-harvesting materials such as quantum dots and porphyrins.[17–23] Moreover, CR was recently demonstrated for photodynamic therapy using titanium dioxide (TiO_2) as an energy receptor.[24] However, the efficiency of the CR activated PDT was low since the radionuclide (^{64}Cu or ^{18}F) was administrated separately from the photosensitizer.

In this study, zirconium-89 (^{89}Zr) with higher energy β emitters (909 keV) and longer half-life ($t_{1/2}$ = 78.4 h) was employed as a CR source to excite chlorin e6 (Ce6) to generate reactive oxygen species (ROS). Ce6 has a strong absorption band peaking at 400 nm, which matches with the CR luminescence of ^{89}Zr. To achieve high energy transfer efficiency, hollow mesoporous silica nanoparticles (HMSNs) were used as a carrier to encapsulate Ce6 molecules and ^{89}Zr isotope, simultaneously. The as-formed nanoconstructs [^{89}Zr]HMSN-Ce6 were found to be efficient in photo-mediated tumor cell destruction, both *in vitro* and *in vivo*. CR from ^{89}Zr was able to transfer its energy to Ce6 nearby to generate enough ROS to cause PDT in tumor cells and tissues. *In vivo* photo-induced therapy was carried out in a murine breast tumor model by subcutaneous injection of [^{89}Zr]HMSN-Ce6 without using any external light source, achieving excellent therapeutic efficacy. At the same time, the radiolabeled [^{89}Zr]HMSN-Ce6 nanoconstruct could also be used for PET image-guided PDT. Thus, our work presents a simplified approach to prepare a multifunctional PET image-guided cancer therapeutic agent with promising potential for future clinical translation.

Synthesis and characterization of [^{89}Zr]HMSN-Ce6

Uniform HMSNs were synthesized following our previous procedure.[25] Figure 1a shows the representative transmission electron microscopy (TEM) image of HMSNs with the size of ~110 nm, and the thickness of HMSNs shell was measured to be ~25 nm. After that, the surface of HMSNs was functionalized with –NH_2 groups with (3-aminopropyl)triethoxysilane (APTES). The resulting HMSN-NH_2 was well-dispersed in water and the hydrodynamic size was measured to be 130 ± 2.1 nm (polydispersity index = 0.09, Figure 1b). The concentration of –NH_2 groups, determined by a Kaiser Test kit was 100 nmol/mL. The amine functionalized HMSNs were then loaded with Ce6 followed by chelator-free radiolabeling with ^{89}Zr. The loading efficiency of Ce6 was measured to be 90 ± 5 % (Figure 2a). After centrifugation and several rounds of washing, the supernatant was just slightly green implying that most of the Ce6 molecules were loaded inside the hollow cavity of HMSN-NH_2 (Figure 2b). Zeta potential of Ce6, HMSN-NH_2 and HMSN-Ce6 in PBS was measured to be −26.6 mV, +9.06 mV and −13.3 mV, respectively, indicating the successful incorporation of Ce6 in HMSN-NH_2. UV-vis-NIR spectra confirmed that HMSNs did not affect the optical properties of Ce6 (Figure 2c). Due to a diffusion gradient, Ce6 slowly diffused out of HMSNs over time at 25 °C as shown in Figure 2d (UV absorbance of Ce6 loaded in HMSN-Ce6 at day 1, 2, 3, 7 and 14 reduces over time). Based on quantitative analysis, Ce6 was released from HMSNs over time in PBS; ~ 9 %, 22 %, 49 % and 56 % at days 2, 3, 7 and 14 respectively.

After loading Ce6 into HMSN-NH_2, ^{89}Zr was intrinsically incorporated in the nanoparticles by chelating with the deprotonated silanol groups on the silica surface to form [^{89}Zr]HMSN-Ce6 nanoconstructs (Figure 2a). Intrinsic labeling of silica nanoparticles (MSNs, bMSNs and dSNs) was previously reported by our group.[26, 27] Here, we applied the same methodology to radiolabel ^{89}Zr on HMSN-Ce6. Briefly, HMSN-Ce6 were incubated with ^{89}Zr (40 MBq, specific activity ~20 GBq μmol^{-1}) in 0.1 M HEPES (4-(2-hydroxyethyl)-1-piperazineethanesulfonicacid) buffer, pH 7–8 for 3 h at 37 °C, with constant vigorous shaking to obtain ~ 40 % labeling yield. In addition, more than ~ 80 %

labeling yield could be obtained by incubating the sample mixture at high temperature (75 °C). Considering that Ce6 rapidly released from the nanoconstructs at high temperatures due to enhanced diffusion, we preferred to perform radiolabeling at 37 °C. Moreover, the [^{89}Zr]HMSN-Ce6 nanoconstruct showed high stability (> 80 %) in mouse serum up to 7 days (Figure 3a).

To further confirm the energy transfer phenomenon, [^{89}Zr]HMSN-Ce6 was imaged using IVIS system with an emission filter 690 – 710 nm to collect only Ce6 emission and the excitation was blocked. Solution containing only ^{89}Zr or HMSN-Ce6 did not emit any signal when using the emission filter (tubes 1&2, Figure 3b) only, while strong fluorescence was observed from solution containing [^{89}Zr]HMSN-Ce6 (tube 3, Figure 3b) indicating that CR from ^{89}Zr could be transferred to Ce6 molecule and emission signal could be obtained without using any external light source.

In vitro CR induced PDT

To determine the efficacy of our nanoconstructs for CR induced PDT, breast cancer cells (4T1) were treated with different concentrations of [^{89}Zr]HMSN-Ce6. Cells treated with [^{89}Zr]HMSN-Ce6 were found to be damaged more than those treated with HMSN-Ce6 only, at the same concentration of Ce6. Moreover, the decrease in cell viability was also found to be Ce6-dose-dependent, when the amount of ^{89}Zr (20 μCi or ~1 MBq) was kept constant; higher amount of Ce6 causing more cell damage (Figure 4a). Interestingly, at 40 μM of Ce6 loaded inside HMSN, the nanoconstructs became toxic to the cells, so 20 μM of Ce6 in HMSN was used to further optimize the dosing regimen with ^{89}Zr. We found that PDT induced killing of 4T1 cells was also dependent on the amount of ^{89}Zr. However, at high radioactivity (50 μCi or ~2 MBq), ^{89}Zr showed some cell toxicity (Figure 4b). Thus, [^{89}Zr]HMSN-Ce6 with 20 μM of Ce6 and 20 μCi of ^{89}Zr were finally chosen for the following cells experiments. Moreover, treatment of [^{89}Zr]HMSN-Ce6 on cancer cells significantly decreased cell viability compared to the cells treated with other controls including ^{89}Zr only, HMSN-NH_2 and HMSN-Ce6 (Figure 4c).

In addition, γ-H_2AX assay based on immunofluorescence microscopy was performed to assess DNA damage in PDT treatment. H_2AX is a variant sequence of histone H_2A that plays an important role in DNA damage response induced by different genotoxic stresses.[28] On exposure to ionizing radiation or chemical agents, chromatin domains around DNA double-stranded breaks (DSBs) in the affected cells are rapidly surrounded by phosphorylated H_2AX (γ-H_2AX). Therefore, γ-H_2AX could be used as a quantitative marker of DSBs in various applications; the detection of γ-H_2AX cores in cell nuclei can be easily done by using immunofluorescence microscopy.[29, 30] As shown in Figure 4d, immunofluorescence images revealed low fluorescent signal of γ-H_2AX in control cells and cells treated with HMSN-Ce6 in the absence of ^{89}Zr, as well as cells incubated with ^{89}Zr. In contrast, the cells cultured in the presence of [^{89}Zr]HMSN-Ce6 nanoconstructs showed a remarkably higher density of γ-H_2AX foci, indicating greater number of DNA double-strand breaks. All collected results reveal the potential of [^{89}Zr]HMSN-Ce6 nanosystem as an effective CR activated PDT.

In vivo Cerenkov radiation induced photodynamic therapy

To demonstrate the *in vivo* applications of Cerenkov radiation induced PDT, a single dose of [^{89}Zr]HMSN-Ce6 (15 MBq, 50 μL) was intratumorally administered into 4T1 tumors in Balb/c mice (average tumor size ~ 200 mm^3). Prolonged tumor retention of [^{89}Zr]HMSN-Ce6 was observed by position emission tomography (PET). Representative maximum intensity projection (MIP) PET images showed that the nanoconstruct was retained inside the tumor area up to 14 observation days (Figure 5a). Moreover, ^{89}Zr remained intact in the HMSNs, as evidenced by very little bone uptake of free ^{89}Zr (^{89}Zr is a well-known osteophilic cation)[31], observed within the experimental time (Figure 5b).

Since highly efficient and stable chelator-free radiolabeling could be achieved with [^{89}Zr]HMSN-Ce6 nanoconstructs, we hypothesized that radiation from even small amounts of radioactivity would efficiently induce Ce6 for PDT over a long period of time. We performed *in vivo* CR induced PDT to confirm the efficacy of our nanoconstruct and observed that tumor growth in mice injected with [^{89}Zr]HMSN-Ce6, 30 μM of Ce6 and 400 μCi of ^{89}Zr in a total volume of 50 μL (n = 4), was completely inhibited within 14 days post injection (p.i., Figure 6). In contrast, the tumors with no injection grew rapidly. Mice injected with [^{89}Zr]HMSN nanoconstructs or HMSN-Ce6 showed tumor growth inhibition initially; yet after day 8 p.i. the tumors growth continued (n = 4, Figure 6). Overall, the percentage reduction in tumor size after 14 days p.i. in mice injected with [^{89}Zr]HMSN-Ce6, [^{89}Zr]HMSN and HMSN-Ce6 was calculated to be 75 %, 20 % and 32 % respectively, relative to the control group. To further understand the effect of CR-induced PDT on tumor tissues, hematoxylin and eosin (H&E) staining was performed on tumor tissue sections, to visualize the apoptosis and resultant morphology of tumor tissues 7 days post-treatment. The results indicated that most of the tumor tissue in the [^{89}Zr]HMSN-Ce6 nanoconstruct group was destroyed, while the tissues in the other three control groups mainly retained their normal morphology (Figure 6d).

Detection of ROS generated in the system was attempted by using various singlet oxygen probes. However, UV based measurement was not successful because CR interfered with the signal. In addition, fluorescence based assay with singlet oxygen sensor green (SOSG) did not give reliable data due to similar concerns. By performing MTT assay with extensive controls, the results suggested that the ROS could be the major factor in destroying the cells. Moreover, detection of the DNA damage via fluorescence cell imaging (Figure 4d) showed the expected outcomes from the treatment group. In addition, after *in vivo* experiment, *ex vivo* histological analysis (Figure 6d) revealed destruction of tumor only in the group exposed to CR induced PDT. Taking all the results together, we conclude that the ROS generated in this system is the key to diminish cell viability.

Our study here demonstrated the innovative concept of new generation PDT agents where external excitation source is not necessary, especially useful for deep-seated tumor therapy. Hollow structures of silica nanoparticles are beneficial for drug loading as well as intrinsically radiolabeling of oxophilic radioisotopes like ^{89}Zr. Unlike the previous study that used CR activated inorganic PS, TiO_2, by injecting the PS nanosystem and radioisotopes separately,[24] our system encapsulated PS and radioisotope in the same nanoconstuct.

One concern that arises from using CR activated PDT is the loss of selectivity since excitation source cannot be focused on only the tumor area as in conventional laser-induced PDT. However, the major advantage of using CR is the treatment of deep-seated tumors and tumors in the regions that external light cannot reach. To overcome the potential drawback, the system needs to be modified and optimized to allow high accumulation in tumor areas but little in the normal tissues, especially in the RES organs, liver and spleen, to avoid side effects of ROS generation from the nanosystem.

Although the intratumoral administration of drugs is a viable therapy for a some tumors, such as hepatocellular (radionuclide therapy through chemoembolization), lung, head and neck or brain cancers,[32–35] intravenous (i.v.) administration of nanomaterials will expand the application of CR induced PDT to a variety of primary and metastatic tumors. However, i.v. injection of nanoparticles usually suffers from high uptake in healthy organs like liver, kidneys and spleen, relative to that in tumors. In this case, decorating the nanomaterials with tumor targeting ligands might help in increasing tumor uptake. Silica nanoparticles have been studied extensively and structure modification with tumor homing ligands have been reported.[36] Recently, biodegradable mesoporous silica nanoparticles (bMSNs) and HMSNs were designed by our group to carry large payloads of drugs (small and large) and functionalized with tumor-specific antibody or small peptides (cRGD) to specifically target the tumor vasculature.[25, 27, 37] Folic acid has also been used to coat the HMSNs surface for tumor targeting purposes, along with imaging dyes and tumor drug (DOX) loaded inside the pores to generate multifunctional nanosystems for cancer imaging and therapy.[38] In addition to avoid the possible side-effects that might occur from uncontrolled ROS generation by CR, proper size of nanoparticles and choice of tumor targeting groups must be selected to allow high accumulation in the tumor in a short period, and reduced accumulation in RES organs at the same time. Bio-distribution of the nanoconstructs needs to be studied carefully to obtain the best system for CR induced PDT.

The focus of the manuscript is to demonstrate an improved concept for enhanced CR-induced PDT of tumors. Since we do not have tumor-targeting groups attached to the nanoconstructs, we did not test the *in vivo* biodistribution of the nanoparticles. Further studies for the surface modification and improvement of the approach are currently underway in our lab. Moreover, based on preliminary PET imaging we can see the injected nanoparticles diffuse from the tumor and end up in the liver and spleen due to uptake by the macrophages, as is well-documented for nanomaterials > 7–10 nm. Further optimization needs to be performed in order to further investigate the CR-mediated PDT effect of these nanoparticles via i.v. administration. At this stage, we would like to initiate the concept of using HMSNs for enhanced CR induced PDT. Overall, promising results from our study indicate the great potential of these nanoconstructs for CR induced PDT, and suggest further improvements needed in the nanoconjugate design to eliminate the current drawbacks.

Conclusions

In summary, we report the first *in vivo* CR induced PDT by using HMSNs. The Ce6 was efficiently loaded into the hollow structure of HMSNs. Intrinsic ^{89}Zr labelling property of HMSNs held the PET radionuclide and PS closed enough to allow efficient energy transfer

process between the components. ^{89}Zr employs high energy β emitters and long half-life which are suitable for long-term photodynamic treatments. Results collected from *in vitro* and *in vivo* experiments confirmed the PDT effects resulting from CR. Tumor targeting with an i.t. administration was suggested to minimize off-target toxicity and offer higher potential for clinical translation. Since CR is low-intensity light, using β emitters with higher energy such as yttrium-90 (2,281 keV) could increase CR intensity and further enhance the PDT effects. Although we focused on the therapy, the approach described here could open up new opportunities to develop better systems to treat a variety of tumors in a depth-independent manner.

Material and Methods

^{89}Zr Production

^{89}Zr-oxalate with a specific activity of >20 GBq/μmol of Zr was isolated and purified according to our previously reported procedures.[39]

Synthesis of HMSN-NH_2

According to the well-established procedures in literature,[25] uniform HMSNs (~ 130 nm) were synthesized by coating the 100 nm sized dSiO_2 nanoparticles with a shell of mesoporous silica, followed by etching away the solid silica core. After that, the as-synthesized HMSNs were surface functionalized with –NH_2 groups and the amine concentration (nmol/mL) was measured using a Kaiser Test kit, Sigma-Aldrich (St. Louis, MO).

Synthesis of HMSN-Ce6

HMSN-NH_2 (0.5 mg) was dispersed in water (pH 5.5, 0.5 mL); then Ce6 (10 mg/mL in DMSO, 50 μL) was added into the solution. The mixture was stirred at 3000 rpm for 24 h. Next, the nanoparticles were centrifuged and washed 3 times with water to remove the unloaded Ce6. The HMSN-Ce6, obtained as a green pellet that was well-dispersed in water, PBS and HEPES buffers.

Characterization

Transmission electron microscopy (TEM) images of the nanoparticles were obtained using a FEI Tecnai TF30 TEM at an acceleration voltage of 300 kV. UV-vis-NIR spectra were collected from a Cary 60 UV-Vis (Agilent Technologies). The hydrodynamic diameters and zeta potential of all nanomaterials were determined by a ZetaSizer Nano-ZS (Malvern Instruments, USA).

Chelator-Free ^{89}Zr Labeling

HMSN-Ce6 in HEPES buffer (pH 7.5; 0.1 M, 0.5 mL) was mixed with 40 MBq ^{89}Zr oxalate. Then, the pH was adjusted to 7.5 – 8 using Na_2CO_3 solution (2 M) before incubation at 37 °C or 75 °C for 3 h. ^{89}Zr labeling yields were monitored by thin layer chromatography (TLC) with 0.05 M EDTA as the mobile phase. Final labeled product was obtained by centrifugation.

Cell Culture Experiment

4T1 murine breast cancer cells were obtained from American Type Culture Collection (ATCC). The cells were cultured in normal RPMI-1640 medium containing 10% fetal bovine serum (FBS) and 1% penicillin/streptomycin at 37 °C under a humidified atmosphere containing 5% CO_2.

In Vitro CR induced Photodynamic Therapy

In a 96-well plate, cells were seeded at a density of 1×10^4 cells per well and incubated with different concentrations of HMSN-Ce6 or [^{89}Zr] HMSN-Ce 6 for 24 h. After removing the culture media, cells were washed twice with PBS. Relative cell viabilities were determined by the standard MTT assay.[40] The OD was measured at 570 nm using SpectraMax Plus 384 microplate reader. Cell viability (%) = (mean of OD of treatment group/mean of OD of control group) × 100.

γ-H2AX Immunofluorescence Analysis

4T1 cells were seeded in 18 mm glass bottom dish (1×10^5 cells per well) and cultured for 24 h. The cells were incubated with HMSN-Ce6, [^{89}Zr]HMSN-Ce6, free Ce6 or free ^{89}Zr (20 μCi) (10 μM of Ce6 in each sample) for 24 h. After incubation, 4% paraformaldehyde was used to fix the cells for 10 min. Then, the cells were rinsed with PBS before permeabilization with methanol at −20 °C, 15 min. Afterward, the cells were washed with PBS before exposure to a blocking buffer (1% BSA in PBS solution) for 1 h at room temperature. Primary antibody (mouse monoclonal anti-phospho-histone γ-H2AX, Biolegend) was then added in a ratio of 1:500 in blocking buffer to incubate with the cells at 4 °C for 24 h. After PBS washing, the cells were incubated with the secondary antibody (donkey anti-mouse Cy3) in a ratio of 1:500 in blocking buffer for another 12 h at 4 °C. Finally, cells were wash thoroughly with PBS and cell nuclei were stained with DAPI before visualizing with a Nikon A1RS Confocal Microscope. Imaging analysis was performed using the NIS-Elements Ar with Deconvolution package.

Tumor Models

All animal studies were conducted under the protocol approved by the University of Wisconsin Institutional Animal Care and Use Committee (IACUC). Subcutaneous xenografts of 4T1 were generated by injection ~50 μL of RPMI-1640 medium containing 1×10^6 cells onto the back of each female Balb/c mice. The mice were used when tumor volumes reached ~200 mm^3.

In Vivo CR Induced PDT

Four groups (n = 4 per group) of mice were randomly divided for various treatments: (i) Control; (ii) HMSN-Ce6; (iii) [^{89}Zr] HMSN and (iv) [^{89}Zr] HMSN-Ce6. Mice were intra-tumorally injected at a dose of 30 μM of Ce6 with 400 μCi of ^{89}Zr (50 μL). The tumor sizes were measured by a caliper every two days and the tumor volumes were calculated as (tumor

length) × (tumor width)^2/2. Seven days after treatment, the tumors from each group were paraffin sections for hematoxylin and eosin (H&E) staining.

Acknowledgments

This work was partly supported by the University of Wisconsin-Madison, the National Institutes of Health (NIBIB/NCI 1R01CA169365, 1R01EB021336, P30CA014520, and T32CA009206), and the American Cancer Society (125246-RSG-13-099-01-CCE).

References

1. Smith AM, Mancini MC, Nie S. Bioimaging: Second Window for in Vivo Imaging. Nat Nanotechnol. 2009; 4:710–711. [PubMed: 19898521]
2. Triesscheijn M, Baas P, Schellens JH, Stewart FA. Photodynamic Therapy in Oncology. Oncologist. 2006; 11:1034–1044. [PubMed: 17030646]
3. Wani S, Puli SR, Shaheen NJ, Westhoff B, Slehria S, Bansal A, Rastogi A, Sayana H, Sharma P. Esophageal Adenocarcinoma in Barrett's Esophagus after Endoscopic Ablative Therapy: A Meta-Analysis Systematic Review. Am J Gastroenterol. 2009; 104:502–513. [PubMed: 19174812]
4. Hsu CY, Chen CW, Yu HP, Lin YF, Lai PS. Bioluminescence Resonance Energy Transfer Using Luciferase-Immobilized Quantum Dots for Self-Illuminated Photodynamic Therapy. Biomaterials. 2013; 34:1204–1212. [PubMed: 23069718]
5. Magalhães CM, Esteves da Silva JCG, Pinto da Silva L. Chemiluminescence and Bioluminescence as an Excitation Source in the Photodynamic Therapy of Cancer: A Critical Review. ChemPhysChem. 2016; 17:2286–2294. [PubMed: 27129132]
6. Cleary K, Peters TM. Image-Guided Interventions: Technology Review and Clinical Applications. Annu Rev Biomed Eng. 2010; 12:119–142. [PubMed: 20415592]
7. Huang Y, He S, Cao W, Cai K, Liang XJ. Biomedical Nanomaterials for Imaging-Guided Cancer Therapy. Nanoscale. 2012; 4:6135–6149. [PubMed: 22929990]
8. Jaffray DA. Image-Guided Radiotherapy: From Current Concept to Future Perspectives. Nat Rev Clin Oncol. 2012; 9:688–699. [PubMed: 23165124]
9. Terreno E, Uggeri F, Aime S. Image Guided Therapy: The Advent of Theranostic Agents. J Control Release. 2012; 161:328–337. [PubMed: 22626940]
10. Cheng L, Wang C, Feng L, Yang K, Liu Z. Functional Nanomaterials for Phototherapies of Cancer. Chem Rev. 2014; 114:10869–10939. [PubMed: 25260098]
11. Wang C, Cheng L, Liu YM, Wang XJ, Ma XX, Deng ZY, Li YG, Liu Z. Imaging-Guided Ph-Sensitive Photodynamic Therapy Using Charge Reversible Upconversion Nanoparticles under near-Infrared Light. Advanced Functional Materials. 2013; 23:3077–3086.
12. Li Z, Wang C, Cheng L, Gong H, Yin S, Gong Q, Li Y, Liu Z. Peg-Functionalized Iron Oxide Nanoclusters Loaded with Chlorin E6 for Targeted, Nir Light Induced, Photodynamic Therapy. Biomaterials. 2013; 34:9160–9170. [PubMed: 24008045]
13. Taratula O, Schumann C, Naleway MA, Pang AJ, Chon KJ, Taratula O. A Multifunctional Theranostic Platform Based on Phthalocyanine-Loaded Dendrimer for Image-Guided Drug Delivery and Photodynamic Therapy. Mol Pharm. 2013; 10:3946–3958. [PubMed: 24020847]
14. Muhanna N, Cui L, Chan H, Burgess L, Jin CS, MacDonald TD, Huynh E, Wang F, Chen J, Irish JC, Zheng G. Multimodal Image-Guided Surgical and Photodynamic Interventions in Head and Neck Cancer: From Primary Tumor to Metastatic Drainage. Clin Cancer Res. 2016; 22:961–970. [PubMed: 26463705]
15. Gambhir SS. Molecular Imaging of Cancer with Positron Emission Tomography. Nat Rev Cancer. 2002; 2:683–693. [PubMed: 12209157]
16. Cherenkov PA. Radiation from High-Speed Particles. Science. 1960; 131:136–142. [PubMed: 13809644]
17. Mitchell GS, Gill RK, Boucher DL, Li C, Cherry SR. In Vivo Cerenkov Luminescence Imaging: A New Tool for Molecular Imaging. Philos Trans A Math Phys Eng Sci. 2011; 369:4605–4619. [PubMed: 22006909]

18. Thorek D, Robertson R, Bacchus WA, Hahn J, Rothberg J, Beattie BJ, Grimm J. Cerenkov Imaging - a New Modality for Molecular Imaging. Am J Nucl Med Mol Imaging. 2012; 2:163–173. [PubMed: 23133811]
19. Liu H, Zhang X, Xing B, Han P, Gambhir SS, Cheng Z. Radiation-Luminescence-Excited Quantum Dots for in Vivo Multiplexed Optical Imaging. Small. 2010; 6:1087. [PubMed: 20473988]
20. Zhang R, D'Souza AV, Gunn JR, Esipova TV, Vinogradov SA, Glaser AK, Jarvis LA, Gladstone DJ, Pogue BW. Cherenkov-Excited Luminescence Scanned Imaging. Opt Lett. 2015; 40:827–830. [PubMed: 25723443]
21. Thorek DL, Riedl CC, Grimm J. Clinical Cerenkov Luminescence Imaging of (18)F-Fdg. J Nucl Med. 2014; 55:95–98. [PubMed: 24078721]
22. Hu H, Cao X, Kang F, Wang M, Lin Y, Liu M, Li S, Yao L, Liang J, Liang J, Nie Y, Chen X, Wang J, Wu K. Feasibility Study of Novel Endoscopic Cerenkov Luminescence Imaging System in Detecting and Quantifying Gastrointestinal Disease: First Human Results. Eur Radiol. 2015; 25:1814–1822. [PubMed: 25577521]
23. Das S, Thorek DL, Grimm J. Cerenkov Imaging. Adv Cancer Res. 2014; 124:213–234. [PubMed: 25287690]
24. Kotagiri N, Sudlow GP, Akers WJ, Achilefu S. Breaking the Depth Dependency of Phototherapy with Cerenkov Radiation and Low-Radiance-Responsive Nanophotosensitizers. Nat Nanotechnol. 2015; 10:370–379. [PubMed: 25751304]
25. Chen F, Hong H, Shi S, Goel S, Valdovinos HF, Hernandez R, Theuer CP, Barnhart TE, Cai W. Engineering of Hollow Mesoporous Silica Nanoparticles for Remarkably Enhanced Tumor Active Targeting Efficacy. Sci Rep. 2014; 4:5080. [PubMed: 24875656]
26. Chen F, Goel S, Valdovinos HF, Luo H, Hernandez R, Barnhart TE, Cai W. In Vivo Integrity and Biological Fate of Chelator-Free Zirconium-89-Labeled Mesoporous Silica Nanoparticles. ACS Nano. 2015; 9:7950–7959. [PubMed: 26213260]
27. Goel S, Chen F, Luan S, Valdovinos HF, Shi S, Graves SA, Ai F, Barnhart TE, Theuer CP, Cai W. Engineering Intrinsically Zirconium-89 Radiolabeled Self-Destructing Mesoporous Silica Nanostructures for in Vivo Biodistribution and Tumor Targeting Studies. Adv Sci. 2016
28. Redon C, Pilch D, Rogakou E, Sedelnikova O, Newrock K, Bonner W. Histone H2a Variants H2ax and H2az. Curr Opin Genet Dev. 2002; 12:162–169. [PubMed: 11893489]
29. Kuo LJ, Yang LX. Gamma-H2ax - a Novel Biomarker for DNA Double-Strand Breaks. In Vivo. 2008; 22:305–309. [PubMed: 18610740]
30. Mah LJ, El-Osta A, Karagiannis TC. Gammah2ax: A Sensitive Molecular Marker of DNA Damage and Repair. Leukemia. 2010; 24:679–686. [PubMed: 20130602]
31. Abou DS, Ku T, Smith-Jones PM. In Vivo Biodistribution and Accumulation of 89zr in Mice. Nucl Med Biol. 2011; 38:675. [PubMed: 21718943]
32. Klutz K, Willhauck MJ, Wunderlich N, Zach C, Anton M, Senekowitsch-Schmidtke R, Goke B, Spitzweg C. Sodium Iodide Symporter (Nis)-Mediated Radionuclide ((131)I, (188)Re) Therapy of Liver Cancer after Transcriptionally Targeted Intratumoral in Vivo Nis Gene Delivery. Hum Gene Ther. 2011; 22:1403–1412. [PubMed: 21488714]
33. Khuri FR, Nemunaitis J, Ganly I, Arseneau J, Tannock IF, Romel L, Gore M, Ironside J, MacDougall RH, Heise C, Randlev B, Gillenwater AM, Bruso P, Kaye SB, Hong WK, Kirn DH. A Controlled Trial of Intratumoral Onyx-015, a Selectively-Replicating Adenovirus, in Combination with Cisplatin and 5-Fluorouracil in Patients with Recurrent Head and Neck Cancer. Nat Med. 2000; 6:879–885. [PubMed: 10932224]
34. Swisher SG, Roth JA, Komaki R, Gu J, Lee JJ, Hicks M, Ro JY, Hong WK, Merritt JA, Ahrar K, Atkinson NE, Correa AM, Dolormente M, Dreiling L, El-Naggar AK, Fossella F, Francisco R, Glisson B, Grammer S, Herbst R, Huaringa A, Kemp B, Khuri FR, Kurie JM, Liao Z, McDonnell TJ, Morice R, Morello F, Munden R, Papadimitrakopoulou V, Pisters KM, Putnam JB Jr, Sarabia AJ, Shelton T, Stevens C, Shin DM, Smythe WR, Vaporciyan AA, Walsh GL, Yin M. Induction of P53-Regulated Genes and Tumor Regression in Lung Cancer Patients after Intratumoral Delivery of Adenoviral P53 (Ingn 201) and Radiation Therapy. Clin Cancer Res. 2003; 9:93–101. [PubMed: 12538456]

35. Yamanaka R, Abe T, Yajima N, Tsuchiya N, Tsuchiya N, Homma J, Kobayashi T, Narita M, Takahashi M, Tanaka R. Vaccination of Recurrent Glioma Patients with Tumour Lysate-Pulsed Dendritic Cells Elicits Immune Responses: Results of a Clinical Phase I/Ii Trial. British Journal of Cancer. 2003; 89:1172–1179. [PubMed: 14520441]

36. Tang F, Li L, Chen D. Mesoporous Silica Nanoparticles: Synthesis, Biocompatibility and Drug Delivery. Adv Mater. 2012; 24:1504–1534. [PubMed: 22378538]

37. Chakravarty R, Goel S, Hong H, Chen F, Valdovinos HF, Hernandez R, Barnhart TE, Cai W. Hollow Mesoporous Silica Nanoparticles for Tumor Vasculature Targeting and Pet Image-Guided Drug Delivery. Nanomedicine (Lond). 2015; 10:1233–1246. [PubMed: 25955122]

38. Yang S, Chen D, Li N, Xu Q, Li H, Gu F, Xie J, Lu J. Hollow Mesoporous Silica Nanocarriers with Multifunctional Capping Agents for in Vivo Cancer Imaging and Therapy. Small. 2016; 12:360–370. [PubMed: 26618618]

39. Zhang Y, Hong H, Severin GW, Engle JW, Yang YA, Goel S, Nathanson AJ, Liu G, Nickles RJ, Leigh BR, Barnhart TE, Cai WB. Immunopet and near-Infrared Fluorescence Imaging of Cd105 Expression Using a Monoclonal Antibody Dual-Labeled with Zr-89 and Irdye 800cw. AmerJ Transl Res. 2012; 4:333. [PubMed: 22937210]

40. Mosmann T. Rapid Colorimetric Assay for Cellular Growth and Survival: Application to Proliferation and Cytotoxicity Assays. J Immunol Methods. 1983; 65:55–63. [PubMed: 6606682]

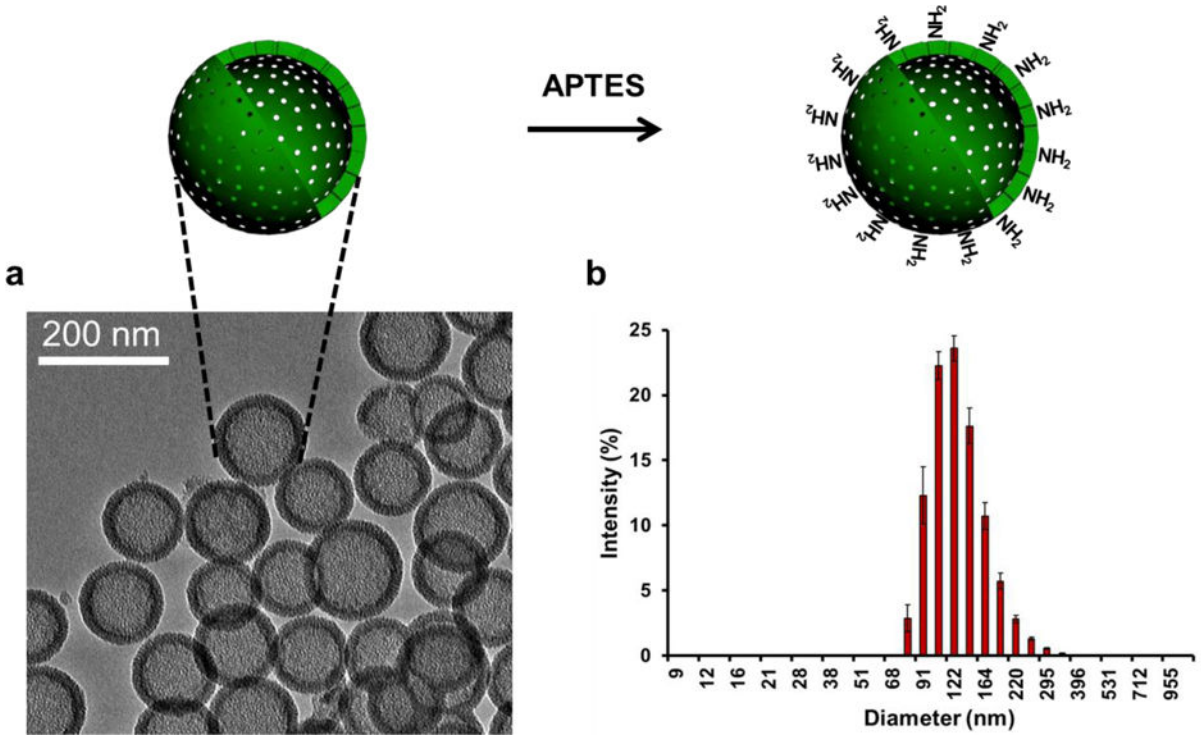

Figure 1.

Physicochemical characterization of HMSNs. (a) TEM image shows an average particle size ~110 nm. (Scale bar: 200 nm) Outset schematic depicts the structure of HMSN showing a hollow cavity with a mesoporous shell. (b) DLS measurements depicting monodispersed hydrodynamic size distribution of HMSN-NH_2 (polydispersity index, PDI = 0.09).

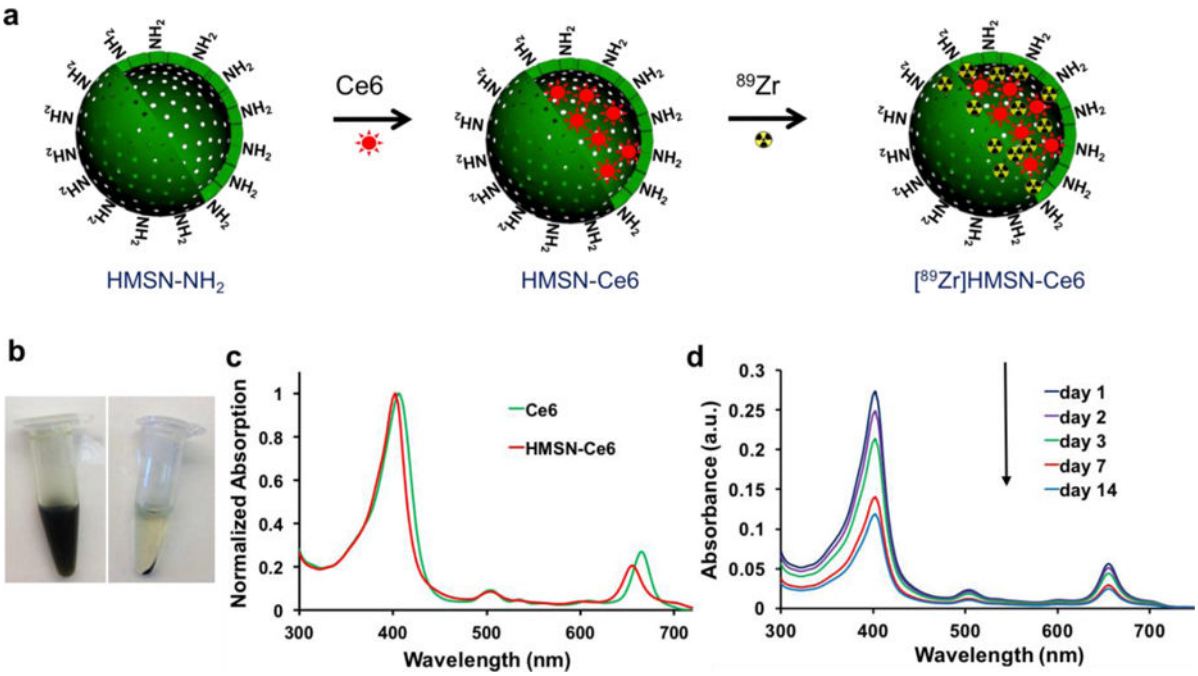

Figure 2.

(a) Schematic represents the synthesis of [^{89}Zr]HMSN-Ce6 nanoconstructs. Ce6 was first loaded inside the hollow structure of HMSN-NH_2 followed by direct chelator-free labeling with oxophilic ^{89}Zr to form [^{89}Zr]HMSN-Ce6. (b) Digital photos of HMSN-Ce6 show nanoparticles in PBS before (left) and after centrifugation (right). (c) UV-vis-NIR spectra of Ce6 and HMSN-Ce6 in PBS (red). (d) Reduction of UV absorbance of Ce6 loaded in HMSN-Ce6 at day 1, 2, 3, 7 and 14, indicating that Ce6 slowly releases from HMSN over time at 25 °C.

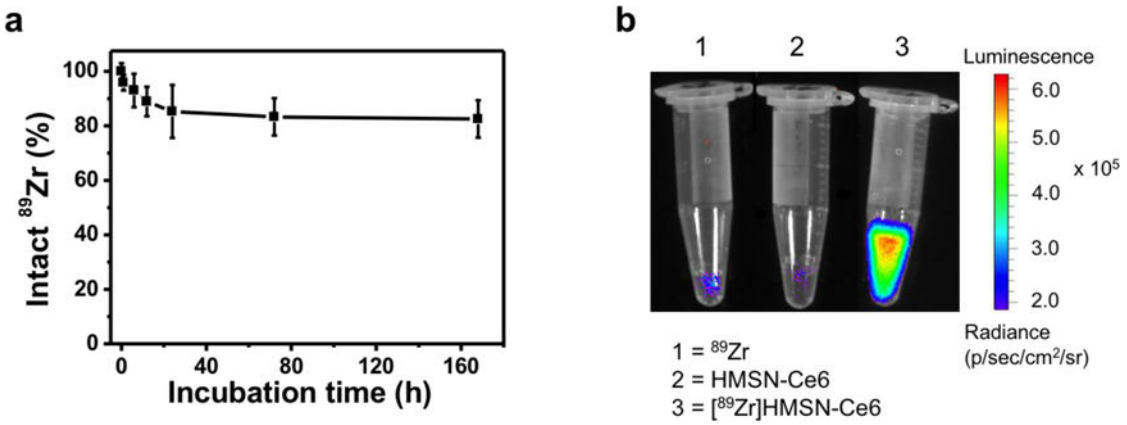

Figure 3.

(a) *In vitro* stability test of [^{89}Zr] HMSN-Ce6 after incubation in mouse serum, at 37 °C for different periods of time. (b) Luminescence imaging of PBS solution containing ^{89}Zr (tube 1), HMSN-Ce6 (tube 2) and [^{89}Zr]HMSN-Ce6 (tube 3). Images were acquired using an IVIS spectrum in vivo imaging system (emission filter 690 – 710 nm, excitation was blocked).

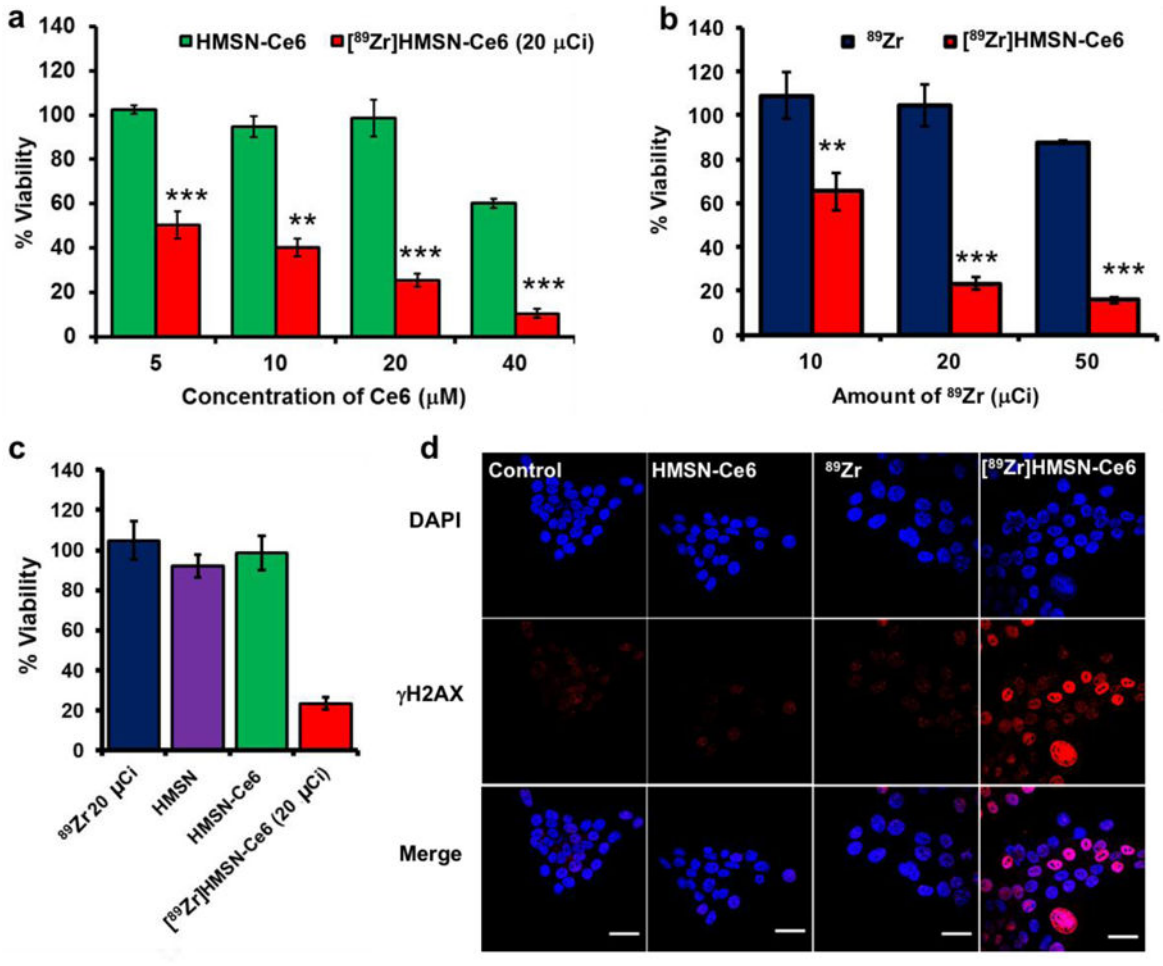

Figure 4.

In vitro Cerenkov radiation induced photodynamic therapy. (a) Cell viability of 4T1 cells treated with various concentrations of Ce6 in HMSN-Ce6 and [^{89}Zr]HMSN-Ce6 nanoconstructs. (b) Cell viability of 4T1 cells treated with various amounts of ^{89}Zr in [^{89}Zr]HMSN-Ce6 nanoconstructs. (c) Cell viability of 4T1 cells treated with ^{89}Zr, HMSNs, HMSN-Ce6 and [^{89}Zr]HMSN-Ce6, the concentrations of Ce6 and HMSNs were kept the same. (d) Confocal images of γ-H_2AX stained 4T1 cells treated with PBS (control), HMSN-Ce6, free ^{89}Zr and [^{89}Zr]HMSN-Ce6 nanoconstructs., scale bar = 20 μm. Error bars represent SD of at least three replicates. P values: ***P < 0.001, ** P<0.01, and *P<0.5.

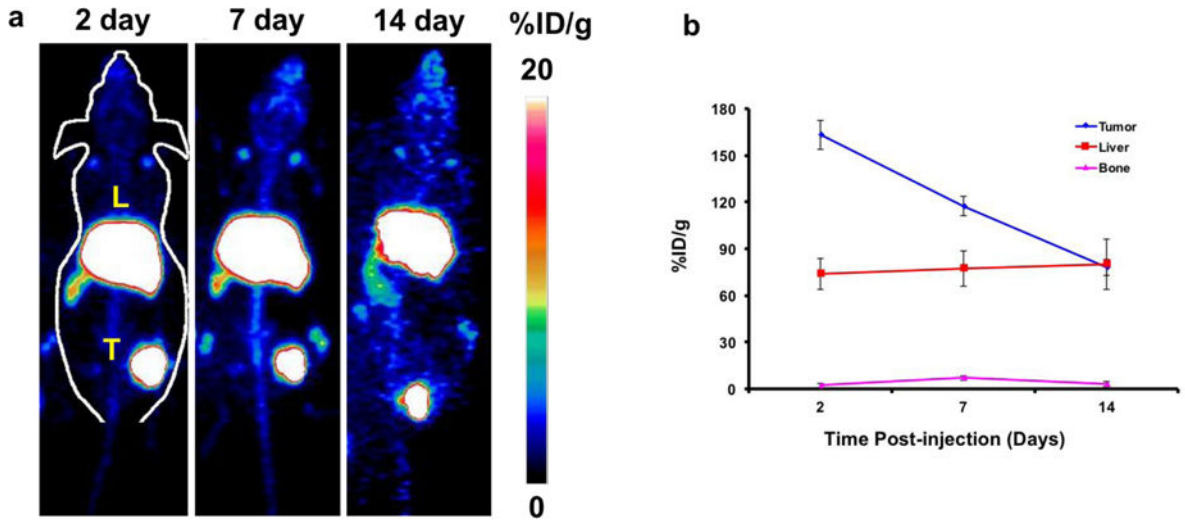

Figure 5.

In vivo PET imaging of [^{89}Zr]HMSN-Ce6. (a) Maximum intensity projection PET images of 4T1 tumor-bearing mice taken at various time points (2, 7 and 14 day) post injection (p.i.) of [^{89}Zr]HMSN-Ce6. (b) Region-of-interest quantification of [^{89}Zr]HMSN-Ce6 uptake in the 4T1 tumor, liver, and bone at various time points p.i. The unit is the percentage of injected dose per gram of tissue (%ID/g). Error bars represent SD of three replicates.

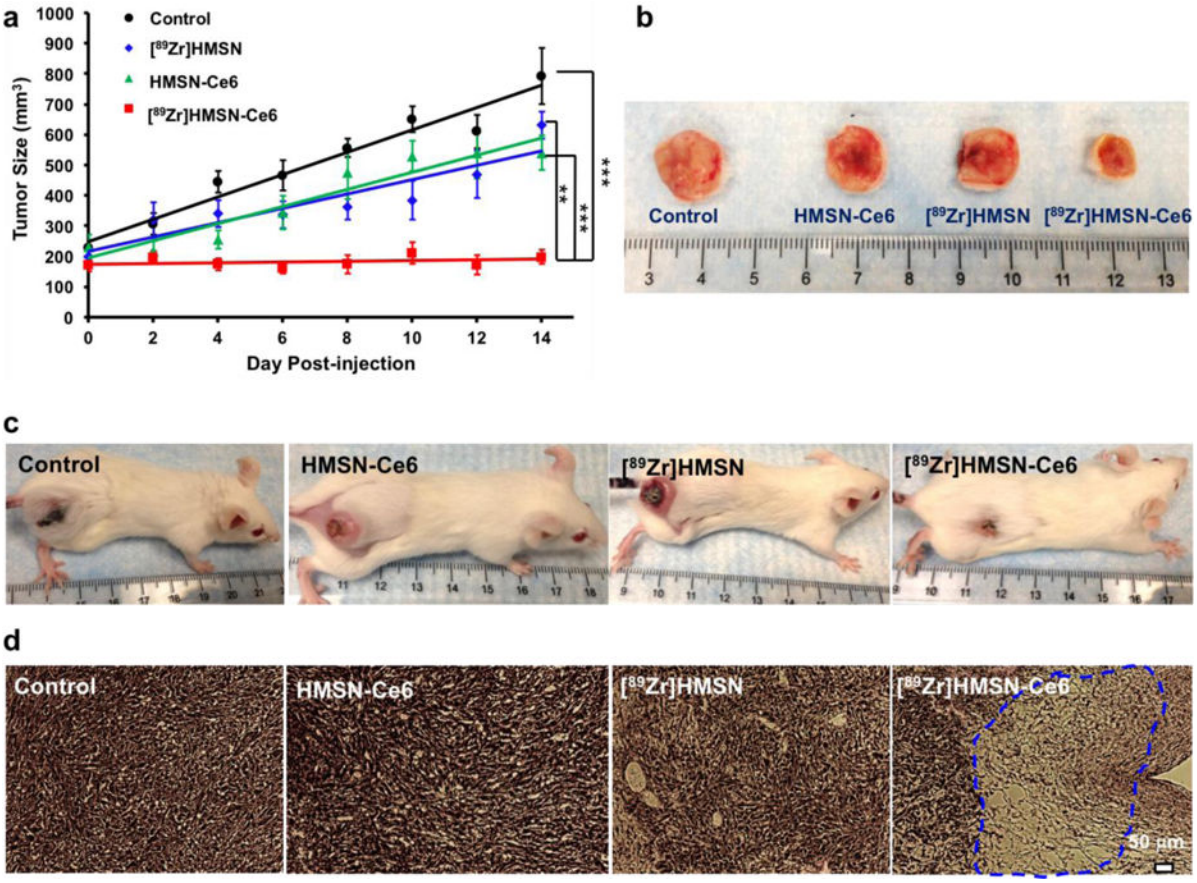

Figure 6.

In vivo Cerenkov radiation induced photodynamic therapy. (a) Tumor growth curves of different groups of mice after various treatments indicated; control group with no injection (black), mice injected with [^{89}Zr]HMSN (blue), HMSN-Ce6 (green) and [^{89}Zr]HMSN-Ce6 (red), n=4. Error bars were based on SD. (b) Representative photographs of tumors from different groups taken at the day 16 p.i. (c) Representative photographs of mice from different groups taken at the day 14 p.i. (d) H&E stained tumor slices collected from different groups of mice day 7 after various treatments. Statistical analysis was calculated by student's T-test (*** $p < 0.001$, **$p < 0.01$, or *$p < 0.05$).